Journal of Science and Technology in Civil Engineering, HUCE, 2025

AXIAL PERFORMANCE OF UHPC-FILLED STEEL TUBE COMPOSITE COLUMNS

Hoang Hieu Nghia[a], Mai Viet Chinh[b,*]

[a]*Faculty of Technology and Engineering, Hai Phong University, 171 Phan Dang Luu road, Phu Lien ward, Hai Phong, Vietnam*
[b]*Institute of Construction Technology, Le Quy Don Technical University, 236 Hoang Quoc Viet road, Nghia Do ward, Ha Noi, Vietnam*

Article history:
Received 24/7/2025, Revised 07/11/2025, Accepted 01/12/2025

Abstract

This study presents a comprehensive finite element investigation into the axial compressive performance of Ultra High Performance Concrete-filled steel tube (UHPC-FST) composite columns. A numerical model is developed using ABAQUS, incorporating nonlinear constitutive models for both steel and UHPC materials. The model is validated using experimental data, demonstrating a strong correlation in terms of load-displacement behavior and ultimate strength. Extensive studies are conducted to evaluate the influence of key design parameters on the axial capacity of UHPC-FST columns. Increasing the steel yield strength from 450 MPa to 750 MPa led to a 1.21-fold increase in axial load capacity. Similarly, raising the UHPC compressive strength from 110 MPa to 190 MPa enhanced the capacity by approximately 1.43 times. A twofold increase in the thickness of the steel tube yielded a modest improvement of about 1.15 times. In contrast, changing the column diameter from 400 mm to 600 mm had the most significant effect, resulting in a 1.97-fold increase in axial capacity. The study also investigates the stress distribution, confirming that the UHPC core and steel shell act synergistically to delay local buckling and failure. The findings demonstrate the significant potential of UHPC-FST composite columns for high-performance structural applications and provide useful insights for future design guidelines.

Keywords: concrete-filled steel tube column; Ultra High Performance Concrete (UHPC); UHPC-FST; axial load; simulation model.

1. Introduction

The increasing demand for high-performance structural systems in contemporary civil engineering, especially in the domains of high-rise construction, transportation infrastructure, and offshore facilities, has catalyzed the development of advanced composite columns. Among these, concrete-filled steel tube columns have attracted considerable interest owing to their superior structural performance, including high load-bearing capacity, favorable ductility, and efficient use of materials [1–7]. These benefits arise from the confinement effect provided by the steel tube and the passive restraint of the core concrete, enabling superior axial performance and energy dissipation capacity compared to conventional reinforced concrete columns.

In recent years, Ultra-High Performance Concrete (UHPC) has emerged as a potential alternative infill material for CFST systems due to its outstanding mechanical and durability properties, such as compressive strength exceeding 120 MPa, dense microstructure, and enhanced resistance to corrosion, impact, and fire [8–15]. When filled into steel tubes, UHPC can synergize with the confining effect of the steel shell to mitigate its intrinsic brittleness, transforming the composite section into a high-performance structural element suitable for critical load-bearing applications [16–20]. Several

*Corresponding author. *E-mail address:* maivietchinh@lqdtu.edu.vn (Chinh, M. V.)

studies have investigated the axial behavior of UHPC-filled steel tube (UHPC-FST) columns through experimental and numerical approaches. Xiong et al. [21] carried out a comprehensive experimental study on CFST columns incorporating ultra-high-strength concrete (up to 190 MPa) and high-strength steel tubes exhibiting yield strengths as high as 780 MPa. Their results demonstrated that current design codes, such as Eurocode 4 [22], often fail to accurately predict the axial resistance of CFSTs when UHPC is used, necessitating modifications to account for the nonlinear interaction effects and confinement mechanisms unique to UHPC. Similarly, Similarly, Chen et al. combined both experimental and finite element methods to investigate the effect of parameters such as fiber content, tube diameter, and steel ratio on the axial strength and ductility of UHPC encased CFST stub columns [23]. Li et al. [24] experimentally investigated UHPC-filled stainless-steel tube columns with coarse aggregates to improve corrosion resistance and performance. Varying parameters showed that higher confinement ratios altered failure modes, and coarse aggregates enhanced stiffness. Eurocode predictions were less accurate at high confinement, indicating the need for better models. Lai et al. [25] experimentally examined UHPC-encased CFST columns (UECCs) under lateral low-velocity impact. Using 12 specimens, they assessed the effects of fiber content, steel tube size, and reinforcement. Results showed that UECCs outperformed conventional columns due to better composite action, with steel fibers and rebar significantly enhancing impact resistance and energy dissipation.

In terms of modeling, the study by Cheng et al. [26] investigates the axial behavior of full-scale UHPC-filled steel tube composite columns (FUCFSTCs) through numerical simulation using ABAQUS, supported by experimental validation. A total of 21 specimens were analyzed, with parameters such as steel strength, tube thickness, and aspect ratio being varied. The numerical model achieved a maximum error of 6.54% compared to test data, demonstrating good predictive accuracy. Cai et al. [27] developed a fiber-based numerical model to analyze the static and dynamic behavior of UHPC-FST columns having rectangular cross section. The model incorporates second-order effects, material nonlinearity, and local buckling, and was validated against experimental results, showing good accuracy in predicting structural performance. Patel et al. performed an axisymmetric simulation to study axially loaded ultra-high strength CFST short columns. Their model, validated against test data, showed that using UHSC could reduce column size by up to 50% [28].

Prior studies focused either on limited experimental configurations or on validating specific design models. Consequently, a systematic numerical framework that can generalize the behavior of UHPC-FST columns across varying configurations is still lacking. This study conducts a comprehensive numerical investigation into the axial compressive behavior of UHPC-filled steel tube composite columns using finite element modeling in ABAQUS. The proposed models are validated against available experimental data and subsequently used to analyze the influence of key parameters, including steel yield strength, UHPC compressive strength, steel tube thickness, and column diamete. It highlights the dominant role of column diameter compared with material over-strengthening, offering practical guidance for structural optimization and supporting potential extensions of current design provisions.

2. Materials and model

2.1. Input parameters for numerical simulation of UHPC-FST columns

Fig. 1 presents the geometric configuration of the UHPC-FST composite columns used in the numerical simulations, including both cross-sectional and longitudinal views. The composite system consists of a circular steel tube enclosing an UHPC core. The outer diameter of the steel tube is denoted as D, while the inner diameter of the concrete core is D_2, and the tube wall thickness is defined as t. The total height of the column is L, which remains constant throughout all parametric

studies. This configuration is intended to simulate realistic confinement conditions in which the steel tube provides lateral restraint to the UHPC core under axial compression. The schematic also reflects typical displacement trends observed in these columns, such as axial shortening and lateral dilation, which are crucial in capturing the composite interaction between the steel shell and the UHPC core. Table 1 summarizes the case matrix and input parameters adopted in the finite element simulations. The study systematically investigates the influence of four key parameters: steel yield strength (f_y), UHPC compressive strength (f_c), steel tube thickness (t), and column diameter (D). The parametric cases are divided into four groups: (1) columns UHPC-FST1 to UHPC-FST4 vary f_y from 450 MPa to 750 MPa while keeping other parameters constant; (2) columns UHPC-FST5 to UHPC-FST8 examine the effect of increasing f_c from 110 MPa to 190 MPa; (3) columns UHPC-FST9 to UHPC-FST12 investigate the effect of t ranging from 12 mm to 20 mm; and (4) columns UHPC-FST13 to UHPC-FST16 explore the influence of increasing D from 400 mm to 600 mm. The reference column, UHPC-FST1, appears in multiple groups to serve as a benchmark for comparison.

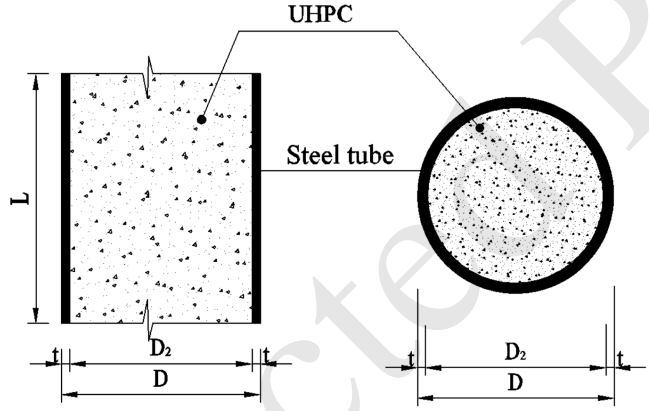

Figure 1. Cross-sectional and longitudinal views of the UHPC-FST column

Table 1. Case studies and input parameters of simulation model

Column number	L (m)	f_c (MPa)	f_y (MPa)	D (mm)	t (mm)
Influence of steel yield strength					
UHPC-FST 1	2500	130	450	400	20
UHPC-FST 2	2500	130	550	400	20
UHPC-FST 3	2500	130	650	400	20
UHPC-FST 4	2500	130	750	400	20
Influence of UHPC's compressive strength					
UHPC-FST 5	2500	110	450	400	20
UHPC-FST 1	2500	130	450	400	20
UHPC-FST 6	2500	150	450	400	20
UHPC-FST 7	2500	170	450	400	20
UHPC-FST 8	2500	190	450	400	20
Influence of steel tube thickness					
UHPC-FST 9	2500	130	450	400	12

Column number	L (m)	f_c (MPa)	f_y (MPa)	D (mm)	t (mm)
UHPC-FST 10	2500	130	450	400	14
UHPC-FST 11	2500	130	450	400	16
UHPC-FST 12	2500	130	450	400	18
UHPC-FST 1	2500	130	450	400	20
Influence of column diameter					
UHPC-FST 1	2500	130	450	400	20
UHPC-FST 13	2500	130	450	450	20
UHPC-FST 14	2500	130	450	500	20
UHPC-FST 15	2500	130	450	550	20
UHPC-FST 16	2500	130	450	600	20

2.2. *Material model*

The steel constitutive model adopted in this study employs a bilinear formulation that incorporates plastic hardening behavior. The model defines the stress–strain relationship using an elastic modulus of 200000 MPa and a Poisson's ratio of 0.3. The mechanical behavior of concrete confined within a steel tube-under axial loading, enters a triaxial stress state, as illustrated in Fig. 2. Using an unconfined concrete model would fail to adequately reflect the actual material behavior under these conditions. Although several nonlinear constitutive models for confined concrete have been developed, such as those by Han [29], Tao [30], and Lam [31], each has limitations in scope. Specifically, Han's model is tailored for normal-strength concrete, while Teng's formulation addresses confinement by GFRP tubes. Given that this study focuses on UHPC confined in steel tubes, the nonlinear concrete model developed by Tao et al. [30] for ultra-high-strength concrete was adopted. The basis relevant formulation for compression and tension behavior are given in Eq. (1):

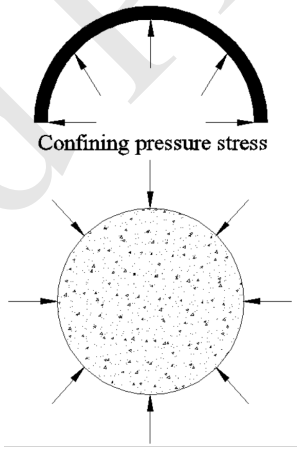

Figure 2. Stress state of concrete

$$\frac{\sigma}{f_c} = \begin{cases} \dfrac{(\mathrm{ax} + bx^2) f_c}{1 + (a-2)x + (b-1)x^2} & (0 < x \leq 1) \\ f_r + (f_c - f_r) \exp\left[-\left(\dfrac{\varepsilon - \varepsilon_{cc}}{\alpha} \right)^{\beta} \right]^2 & (\varepsilon > \varepsilon_{cc}) \end{cases} \tag{1}$$

In Eq. (1), f_r denotes the residual stress, while f_c refers to the maximum compressive strength of the concrete. The parameter β, set to 1.2 for circular steel tube confinement, serves as a confinement coefficient. Additionally, ε_0 indicates the strain value at which the peak compressive stress occurs.

2.3. *Simulation model build-up*

The study developed a finite element (FE) model of a full-scale UHPC-FST subjected to axial loading, using the commercial FE software ABAQUS. The model incorporated eight-node 3D solid

elements (C3D8R) to simulate the behavior of the UHPC and steel elements. Two reference points (RP-1 and RP-2) were assigned to the top and bottom ends of the model and connected to the respective faces of the column. A displacement load was applied at RP-1, with all translational and rotational degrees of freedom fixed at this point. At RP-2, the constraints were more comprehensive, fully restraining translation and rotation in all directions (U_x, U_y, U_z, U_{rx}, U_{ry}, U_{rz}). Here, U_x, U_y, and U_z represent the displacements, while UR_x, UR_y, and UR_z denote the rotational movements about the x, y, and z-axes, respectively. A mesh convergence analysis was conducted using various element sizes, and the results indicated that a mesh size of 15 mm provided an optimal balance between computational efficiency and model accuracy, as illustrated in Fig. 3. Contact interaction between the steel tube and the concrete core was modeled as hard contact in the normal direction, and a tangential penalty friction coefficient of 0.8 was applied to simulate interface behavior.

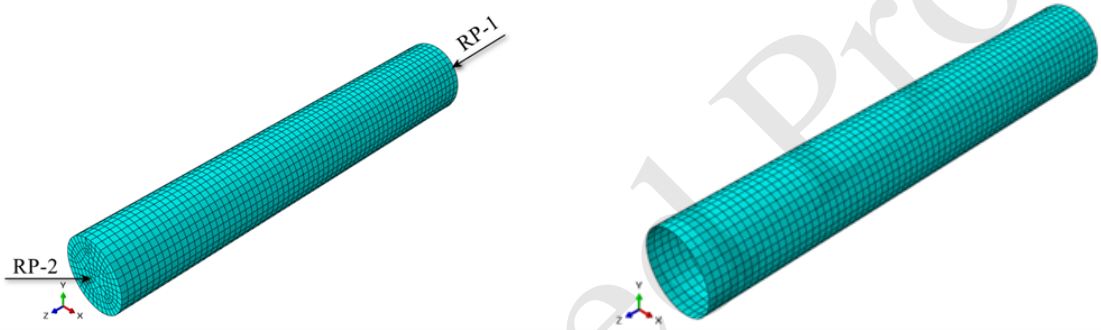

(a) UHPC part (b) Steel part

Figure 3. Mesh model of the UHPC-FST column

3. Results and discussion

3.1. Simulation model validation

To ensure the reliability of the proposed finite element model, a validation was performed by comparing the simulation results with experimental data from UHPC-filled steel tube columns tested by Chen [32]. As presented in Table 2, two specimens of CSC1-2 and CSC1-3 were examined, both having an outer diameter of 113.7 mm and a height of 342 mm. The wall thicknesses were 2.06 mm and 2.05 mm, respectively. The UHPC used in these tests exhibited compressive strengths of 113.2 MPa and 130.8 MPa, while the steel tube had a consistent yield strength of 269.9 MPa.

Table 2. Material parameters used in the tests conducted by Chen [32]

Specimens	D (mm)	t (mm)	f_c (MPa)	f_y (MPa)	L (mm)
CSC1-2	113.7	2.06	113.2	269.9	342
CSC1-3	113.7	2.05	130.8	269.9	342

Based on the comparison between the experimental and numerical results presented in Fig. 4 and Table 3, it can be observed that the finite element model exhibits a good predictive capability in simulating the structural behavior of UHPC-FST columns under axial compression. The load–displacement curves of the CSC1-2 and CSC1-3 columns reveal similar overall trends between the test results and simulations. Both curves show a rapid initial stiffness followed by a peak load and a descending branch, which is consistent with typical UHPC confinement responses. The numerical model captures the general shape of the load–displacement response after peak load, including the softening

Table 3. Comparison of ultimate load between Chen's test [32] and numerical simulation

Case study	Maximum load (kN)	
	CSC1-2	CSC1-3
Test (T)	1487	1535
Simulation (S)	1650.2	1702.7
Disparity (S/T)	1.1	1.11

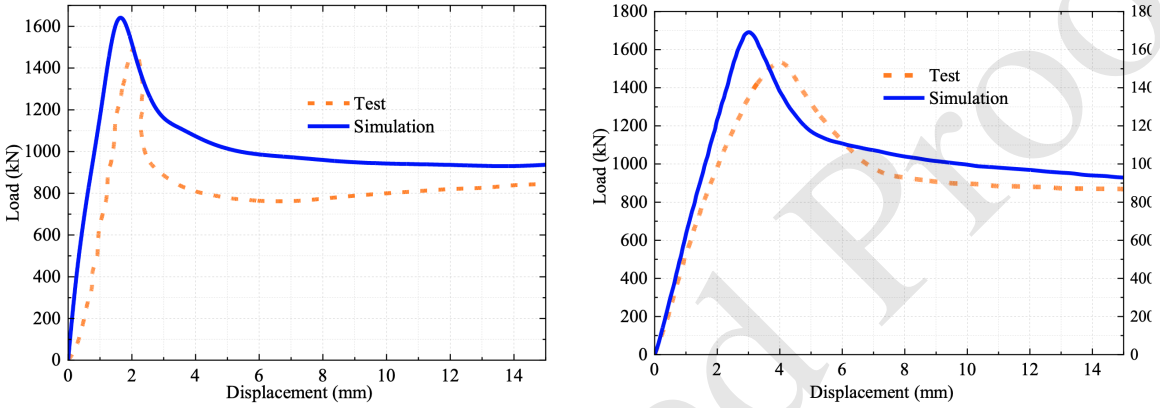

(a) CSC1-2 (b) CSC1-3

Figure 4. Load–displacement curves of UHPC-FST column from Chen's test [32] and simulation

trend associated with UHPC crushing and steel yielding. However, as seen in Fig. 4(a) (CSC1-2), the test shows a sharper drop after the peak, while the simulation exhibits a more gradual decline. This mismatch arises primarily because the FE model assumes uniform material degradation, whereas in reality, UHPC failure involves progressive cracking, fiber pull-out, and localized crushing, which provide faster post-peak response. In contrast, for CSC1-3 (Fig. 4(b)), the agreement between simulation and experiment in the post-peak region is closer, suggesting that the adopted constitutive models are capable of reproducing the nonlinear behavior reasonably well. As indicated in Table 3, the ultimate load obtained from the experiment for CSC1-2 is 1487 kN, whereas the simulation result is 1650.2 kN, yielding a ratio of 1.1. For CSC1-3, the experimental value is 1535 kN while the simulation predicts 1702.7 kN, giving a ratio of 1.11. These differences, though present, remain within a reasonable range (less than 12%), demonstrating the robustness of the simulation model, especially considering the complex interaction between UHPC and steel tube confinement, as well as potential test uncertainties. The slight overestimation can be attributed to the idealized assumptions inherent in the finite element modeling approach. These include perfect material homogeneity in the simulation, the absence of microcracking in UHPC, and the exclusion of initial imperfections in the steel tube, as well as simplifications in boundary conditions. These factors typically lead to a higher modeled stiffness compared to physical test specimens. Nonetheless, the consistency of the simulation in capturing both the stiffness and post-peak behavior validates the selected constitutive models and boundary conditions applied in ABAQUS. Additionally, the load–displacement curves in Fig. 4 confirm the ability of the numerical model to reproduce the entire nonlinear response of the composite column, including the softening behavior after the peak load. The transition from elastic to plastic response, followed by strain softening, is captured with reasonable accuracy, which is essential for

applications involving structural damage prediction or performance-based design. The good agreement between test and simulation results demonstrates the reliability of the adopted finite element model in simulating UHPC-FST column behavior under axial loads. This confirms that the selected material parameters and boundary conditions are suitable for capturing the mechanical response of such composite systems, and the model can be applied for further parametric studies.

3.2. Extensive parametric studies

Following the validation of the proposed numerical model, in this section, extended parametric studies is conducted to examine the influence of key parameters on the axial load-carrying capacity of UHPC-filled steel tube composite columns. The investigated parameters include steel yield strength, UHPC compressive strength, steel tube thickness, and column diameter.

a. Influence of steel yield strength

Based on Table 4 and Fig. 5, the influence of steel yield strength on the axial compressive performance of UHPC-FST columns is examined in detail. The results reveal a clear trend that increasing the yield strength of the steel tube enhances the axial load-carrying capacity of the composite column. As shown in Table 4, all columns have the same geometric and material parameters except for the steel yield strength (f_y), which ranges from 450 MPa to 750 MPa. The column with the lowest steel yield strength (UHPC-FST1, f_y = 450 MPa) exhibits an ultimate axial load (N_u) of 27003.6 kN. When the steel yield strength increases to 550 MPa (UHPC-FST2), N_u rises to 28928.9 kN, yielding a load ratio of 1.07 relative to the reference column. Further increasing f_y to 650 MPa and 750 MPa results in N_u values of 30818.1 kN and 32578.5 kN, corresponding to load ratios of 1.14 and 1.21, respectively. Although the yield strength of the steel increases by 1.67 times (from 450 MPa to 750 MPa), the ultimate axial load only increases by 1.21 times, suggesting a diminishing rate of improvement due to the nonlinear contribution of the steel confinement. These findings indicate a nonlinear but consistent enhancement in load-bearing capacity with increasing f_y. This is attributed to the greater confinement effect and higher stiffness provided by stronger steel tubes, which better restrain the lateral expansion of the UHPC core and delay the onset of local buckling and plastic displacements in the steel shell. Fig. 5 further supports these conclusions by presenting the load–displacement curves for the different f_y values. All curves exhibit similar initial stiffness and peak behavior, but columns with higher f_y not only achieve greater peak loads but also sustain higher post-peak loads. This reflects an improvement in both strength and ductility. The load–displacement curve of UHPC-FST4 (f_y = 750 MPa) demonstrates the most stable post-peak response, indicating a delayed stiffness degradation. Conversely, UHPC-FST1 (f_y = 450 MPa) shows the lowest peak and the lowest pronounced softening behavior.

Table 4. Parameters and results on the influence of steel strength on the axial loading capacity of UHPC-FST columns

Column	L (m)	f_c (MPa)	f_y (MPa)	D (mm)	t (mm)	N_u (kN)	Increment ratio	Note
UHPC-FST 1	2500	130	450	400	20	27003.6	//	//
UHPC-FST 2	2500	130	550	400	20	28928.9	1.07	(2)/(1)
UHPC-FST 3	2500	130	650	400	20	30818.1	1.14	(3)/(1)
UHPC-FST 4	2500	130	750	400	20	32578.5	1.21	(4)/(1)

(N_u: Ultimate axial load)

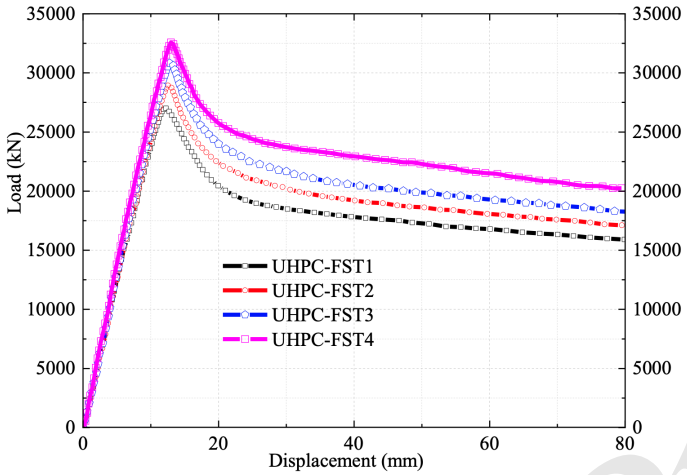

Figure 5. Load-displacement curves of the column under varying steel yield strengths

b. Influence of UHPC's compressive strength

Table 5 and Fig. 6 show the effect of UHPC compressive strength on the axial performance of UHPC-FST composite columns. All columns are designed with identical geometric dimensions and steel yield strength (450 MPa), while the UHPC compressive strength (f_c) is varied from 110 MPa to 190 MPa. The reference column (UHPC-FST5) with f_c = 110 MPa achieves an ultimate axial load (N_u) of 24670.7 kN. When f_c is increased to 130 MPa (UHPC-FST1), N_u rises to 27003.6 kN, corresponding to an increment ratio of 1.09. Further increasing f_c to 150 MPa, 170 MPa, and 190 MPa results in N_u values of 29839.8 kN, 32253.1 kN, and 35344.5 kN, with increment ratios of 1.21, 1.31, and 1.43, respectively. These results highlight a consistent and significant improvement in axial resistance as the compressive strength of UHPC increases. Specifically, increasing f_c by 1.73 times (from 110 MPa to 190 MPa) leads to a 1.43-fold increase in axial capacity, demonstrating the highly beneficial role of high-strength concrete in composite column performance. The enhancement in load-carrying capacity with increasing f_c can be attributed to several key factors. Higher compressive strength of UHPC contributes to greater confinement stiffness and improved interaction between the steel tube and concrete core. It also delays the initiation of crushing and plastic displacement within the concrete, allowing the composite section to sustain higher axial loads prior to failure. Additionally, UHPC with higher compressive strength typically exhibits a denser matrix and better bond performance with the steel tube, which further contributes to improved load transfer and reduced risk of interface debonding or local crushing.

Table 5. Parameters and results on the influence of UHPC's compressive strength on axial loading capacity of UHPC-FST columns

Column	L (m)	f_c (MPa)	f_y (MPa)	D (mm)	t (mm)	N_u (kN)	Increment ratio	Note
UHPC-FST 5	2500	110	450	400	20	24670.7	//	//
UHPC-FST 1	2500	130	450	400	20	27003.6	1.09	(1)/(5)
UHPC-FST 6	2500	150	450	400	20	29839.8	1.21	(6)/(5)
UHPC-FST 7	2500	170	450	400	20	32253.1	1.31	(7)/(5)
UHPC-FST 8	2500	190	450	400	20	35344.5	1.43	(8)/(5)

Fig. 6 illustrates the load–displacement behavior of the columns under different concrete strengths. It can be observed that all columns share similar initial stiffness characteristics, but the peak load

values and post-peak responses differ notably. Columns with higher compressive strength exhibit significantly greater peak loads. However, they tend to experience a more rapid post-peak strength degradation. This trend is evident in UHPC-FST8 (f_c = 190 MPa), which achieves the highest ultimate axial load among all columns but also displays a steeper descending branch after peak, indicating a more brittle failure mode. In contrast, UHPC-FST5 (f_c = 110 MPa) shows the lowest peak load yet exhibits a more gradual reduction in load-carrying capacity after reaching the maximum, suggesting comparatively better ductility. This behavior can be attributed to the inherent material characteristics of concrete, including UHPC, wherein increasing compressive strength is generally accompanied by a reduction in ductility. As the concrete matrix becomes denser and stronger, its ability to undergo inelastic displacement before failure diminishes, leading to a more brittle response.

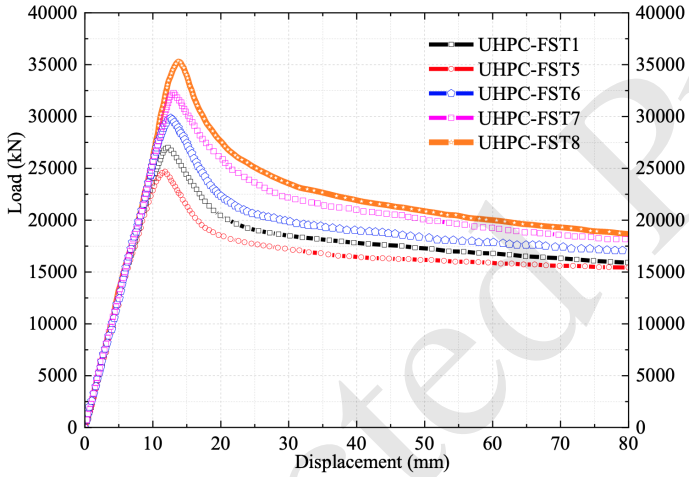

Figure 6. Load-displacement curves of the column under varying UHPC's compressive strengths

c. Influence of steel tube thickness

Table 6 and Fig. 7 provide the basis for evaluating how variations in steel tube thickness affect the axial compressive performance of UHPC-FST composite columns. In this parametric study, all columns are designed with identical geometry and material properties, except for the thickness of the steel tube (t), which varies from 12 mm to 20 mm. As observed, increasing the wall thickness of the steel tube leads to an enhancement in the ultimate axial load. Specifically, the reference column UHPC-FST9 with a thickness of 12 mm achieves a N_u of 23433.9 kN. As the thickness increases to 14 mm (UHPC-FST10), 16 mm (UHPC-FST11), 18 mm (UHPC-FST12), and 20 mm (UHPC-FST1), the corresponding N_u values are 24472.5 kN, 25203.1 kN, 26202.7 kN, and 27003.6 kN, reflecting incremental ratios of 1.04, 1.08, 1.12, and 1.15, respectively, compared to UHPC-FST9. These results suggest that while thicker steel tubes do improve the axial load-bearing capacity, the magnitude of this improvement is relatively modest. In particular, the total increase in N_u from 12 mm to 20 mm thickness is approximately 15%, which is significantly lower than the enhancement observed from varying concrete compressive strength or steel yield strength in the previous parametric studies. This indicates that the axial strength of UHPC-FST columns is less sensitive to changes in steel tube thickness than to changes in material strength parameters. Fig. 7 further illustrates the load–displacement behavior for the different tube thicknesses. All curves exhibit similar initial stiffness and peak shapes, but columns with thicker steel tubes reach higher peak loads and exhibit slightly improved post-peak performance. The post-peak descending branches remain steep across all columns, with only minor differences, implying that increasing steel tube thickness primarily

contributes to load capacity rather than displacement capacity. This behavior can be explained by the fact that thicker steel tubes provide a higher confinement effect and delay local buckling of the shell, which slightly improves load resistance. However, since the confinement efficiency of a circular steel tube is also governed by the strength and stiffness of the UHPC core, and the hoop stress developed during axial loading, the influence of tube thickness becomes secondary when compared with the dominant material properties. Therefore, the overall impact of increasing tube thickness is limited in improving the global axial compressive performance of UHPC-FST columns.

Table 6. Parameters and results on the influence of steel tube thickness on axial loading capacity of UHPC-FST columns

Column	L (m)	f_c (MPa)	f_y (MPa)	D (mm)	t (mm)	N_u (kN)	Increment ratio	Note
UHPC-FST 9	2500	130	450	400	12	23433.9	//	//
UHPC-FST 10	2500	130	450	400	14	24472.5	1.04	(10)/(9)
UHPC-FST 11	2500	130	450	400	16	25203.1	1.08	(11)/(9)
UHPC-FST 12	2500	130	450	400	18	26202.7	1.12	(12)/(9)
UHPC-FST 1	2500	130	450	400	20	27003.6	1.15	(1)/(9)

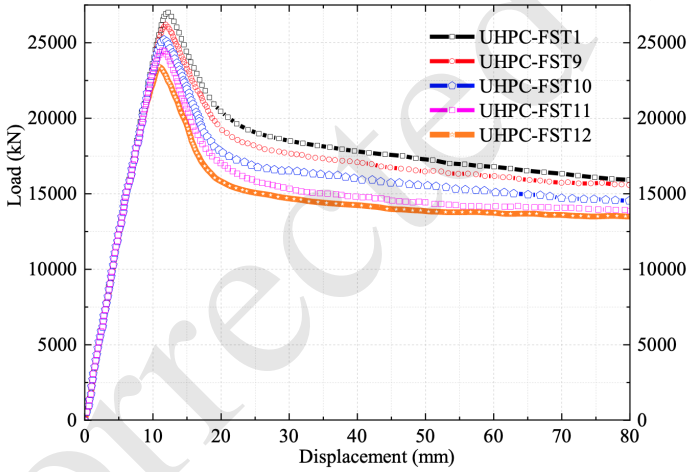

Figure 7. Load-displacement curves of the column under varying steel tube thickness

d. Influence of column diameter

Table 7 and Fig. 8 serve as the basis for a detailed investigation into the axial compressive performance of UHPC-FST composite columns with varying column diameters. All columns share identical material properties (concrete compressive strength of 130 MPa and steel yield strength of 450 MPa) and steel tube thickness (20 mm), with the only parameter varied being the column diameter, ranging from 400 mm to 600 mm. The results demonstrate a clear and substantial improvement in the axial load-carrying capacity with increasing column diameter. Specifically, the column with a 400 mm diameter (UHPC-FST1) achieves an ultimate axial load (N_u) of 27003.6 kN. As the diameter increases to 450 mm (UHPC-FST13), 500 mm (UHPC-FST14), 550 mm (UHPC-FST15), and 600 mm (UHPC-FST16), the ultimate loads rise significantly to 32793.1 kN, 39558.6 kN, 46085.4 kN, and 53248.9 kN, respectively. These correspond to increase ratios of 1.21, 1.46, 1.71, and 1.97, relative to the baseline case. This nearly twofold increase in axial capacity with a 1.5× increase in diameter

(from 400 mm to 600 mm) highlights the dominant role of cross-sectional area in resisting compressive loads. The amplified confinement effect due to the larger volume of UHPC and the improved composite interaction between the steel tube and the concrete core contribute significantly to this enhancement. Moreover, larger diameter columns provide a greater second moment of area, which helps delay global instability and local buckling. Compared to other parameters such as steel yield strength, UHPC compressive strength, or tube thickness, the influence of column diameter is markedly superior. While those parameters enhanced axial performance to varying degrees (with maximum increase ratios of 1.21 for steel yield strength, 1.43 for UHPC strength, and 1.15 for tube thickness), the variation in diameter achieved an increase ratio of up to 1.97. This clearly demonstrates that enlarging the column's cross-section is the most effective means to enhance the load-bearing performance of UHPC-FST composite columns. The load–displacement curves in Fig. 8 reinforces these findings. All columns exhibit similar initial stiffness trends, but those with larger diameters reach substantially higher peak loads and maintain relatively stable post-peak responses. UHPC-FST16 (D = 600 mm) not only shows the highest strength but also sustains load over a longer displacement range, indicating improved ductility and energy dissipation. Conversely, the curve of UHPC-FST1 (D = 400 mm) displays the lowest peak and the steepest softening behavior, confirming its limited structural performance.

Table 7. Parameters and results on the influence of column diameter on axial loading capacity of UHPC-FST columns

Column	L (m)	f_c (MPa)	f_y (MPa)	D (mm)	t (mm)	N_u (kN)	Increment ratio	Note
UHPC-FST 1	2500	130	450	400	20	27003.6	//	//
UHPC-FST 13	2500	130	450	450	20	32793.1	1.21	(13)/(1)
UHPC-FST 14	2500	130	450	500	20	39558.6	1.46	(14)/(1)
UHPC-FST 15	2500	130	450	550	20	46085.4	1.71	(15)/(1)
UHPC-FST 16	2500	130	450	600	20	53248.9	1.97	(16)/(1)

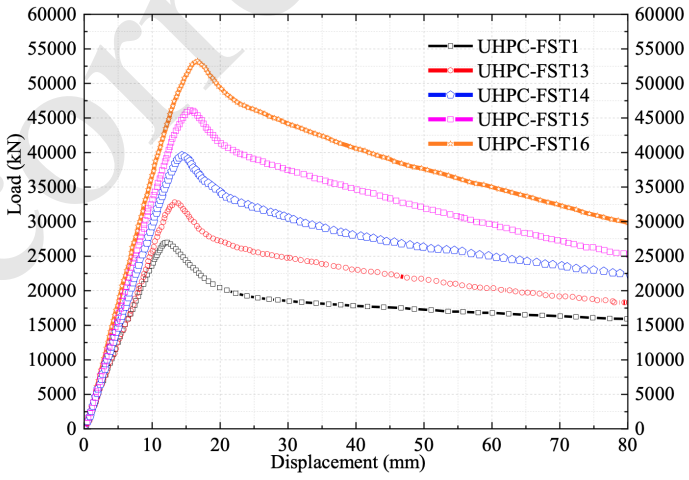

Figure 8. Load-displacement curves of the column under varying column diameter

e. Stress and overall deformation of UHPC-FST columns

The stress contours presented in Figs. 9, 10 illustrate the axial compression behavior of UHPC-FST composite columns. In Fig. 9, the column undergoes a typical compressive mode of displace-

ment, with the maximum displacement occurring at the top loading point and gradually decreasing toward the fixed base. The distribution pattern is largely uniform along the central axis, suggesting that the loading conditions and boundary constraints were properly applied in the FE model. Notably, slight lateral bulging can be observed near the mid-height and lower quarter of the steel tube, indicative of local instability and potential onset of outward expansion of the steel shell due to the internal confinement pressure from the UHPC core. This behavior aligns with experimental observations in full-scale UHPC-FST columns where high-strength UHPC generates significant internal pressure under compression, contributing to confinement-induced outward displacements of the steel tube. Fig. 10 shows the von Mises stress distribution, revealing the internal stress evolution within the steel tube. High stress concentrations are observed near the mid-height region and toward the ends of the column, with peak von Mises stresses approaching the yield limit of the steel material. This indicates that the steel tube has entered the plastic yield stage, particularly in the mid-span regions where outward displacement and local instability are most prominent. These stress zones suggest that the steel tube plays a dominant load-resisting role and enters the plastic regime during peak loading stages. The gradual stress gradient along the height of the column indicates a well-distributed axial force transfer from the loading point through the steel shell to the UHPC core. Furthermore, localized stress peaks at the interface between the tube and UHPC suggest frictional interaction and shear transfer at the steel–concrete interface.

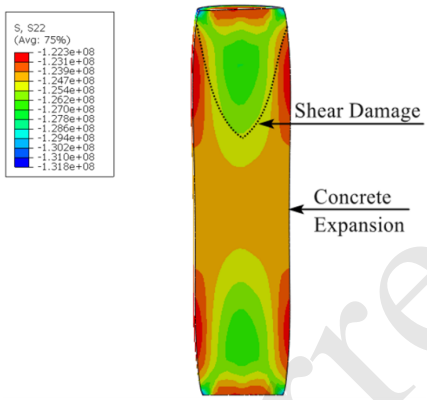

Figure 9. Stress contour of UHPC

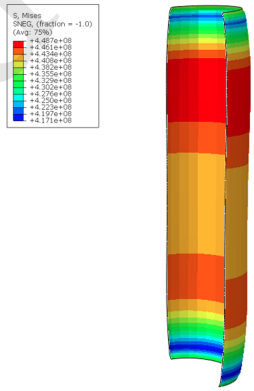

Figure 10. Stress contour of steel tube

In addition, Fig. 9 highlights a distinct region of shear damage initiation near the upper portion of the UHPC core. This is evidenced by the diagonal contour pattern, marked as "Shear Damage", which reflects the onset of internal cracking due to a combination of high axial compression and lateral dilation. The presence of this inclined failure band suggests that the UHPC experiences triaxial stress conditions leading to shear localization, which typically precedes crushing failure in high-strength concrete. The stress contour (S22) in the UHPC core also reveals that compressive stresses approach or reach the material's peak compressive strength, as indicated by the darkest red regions exceeding -1.31×10^8 Pa (In compression). This confirms that the UHPC core has fully mobilized its axial load capacity prior to damage propagation. When cross-referenced with the findings of Cheng et al. (2023) [26], the observed displacement and stress responses are consistent with the described confinement mechanisms of UHPC within steel tubes. The composite interaction delays local buckling of the steel and restrains the brittle failure of UHPC, allowing the column to maintain a stable post-peak response. The residual stress contours in the lower third of the column also point to the energy dissipation capacity of the system, which is a characteristic advantage of UHPC-FST composite systems over conventional RC designs. It is also evident that failure localization begins from mid-height, a

phenomenon reported in the referenced study, which is associated with the concentration of compressive strain and the initiation of cracking or crushing in the UHPC core. This displacement pattern confirms the validity of the nonlinear confined concrete model used in the simulation.

4. Conclusions

This study has numerically examined the axial compressive behavior of UHPC-filled steel tube (UHPC-FST) composite columns through a calibrated finite element model in ABAQUS. The following conclusions are drawn based on the simulation outcomes:

- The proposed FE model accurately replicates experimental results in terms of load–displacement curves, ultimate capacity, confirming its reliability for simulating UHPC-FST columns under axial loading. This validated model can serve as a tool for performance-based design.

- Column diameter has the strongest influence on axial capacity. Increasing steel yield strength, UHPC compressive strength, or tube thickness yields only moderate improvements, with diminishing benefits at higher strength levels and a tendency toward more brittle post-peak behavior in UHPC.

- Stress and displacement analyses show no local buckling, but indicate steel yielding and concrete crushing at peak load. Shear failure zones and confinement effects are evident in later loading stages.

References

[1] Debnath, P. P., Xu, F., Chan, T.-M. (2023). Load transfer mechanism in concrete-filled steel tubular columns: Developments, challenges and opportunities. *Journal of Constructional Steel Research*, 203: 107781.

[2] George, C., Selvan, S. S., Kumar, V. S., Murali, G., Giri, J., Makki, E., Sathish, T. (2024). Enhancing the fire-resistant performance of concrete-filled steel tube columns with steel fiber-reinforced concrete. *Case Studies in Construction Materials*, 20:e02741.

[3] Hu, H.-S., Yang, Z.-J., Xu, L., Zhang, Y.-X., Gao, Y.-C. (2023). Axial compressive behavior of square concrete-filled steel tube columns with high-strength steel fiber-reinforced concrete. *Engineering Structures*, 285:116047.

[4] Luo, X., Yu, X., Wei, J., Jiang, C., Yang, Y. (2025). Mechanical response of slender ultra-high-strength concrete filled high-strength steel tube columns under eccentric compression. *Case Studies in Construction Materials*, 22:e04762.

[5] Miao, K., Wei, Y., Dong, F., Zheng, K., Wang, J. (2023). Experimental study on concrete-filled steel tube columns with inner distributed seawater and sea sand concrete-filled fiber-reinforced polymer tubes under axial compression. *Composite Structures*, 320:117181.

[6] Niyirora, R., Niyonyungu, F., Hakuzweyezu, T., Masengesho, E., Nyirandayisabye, R., Munyaneza, J. (2023). Behavior of concrete-encased concrete-filled steel tube columns under diverse loading conditions: A review of current trends and future prospects. *Cogent Engineering*, 10(1):2156056.

[7] Zhao, C., Li, Y., Lu, Q. (2022). Study on seismic performance of honeycomb stiffened rib shaped concrete filled steel tube columns. *Case Studies in Construction Materials*, 17:e01534.

[8] Abdellatief, M., Al-Tam, S. M., Elemam, W. E., Alanazi, H., Elgendy, G. M., Tahwia, A. M. (2023). Development of ultra-high-performance concrete with low environmental impact integrated with metakaolin and industrial wastes. *Case Studies in Construction Materials*, 18:e01724.

[9] Chinh, M. V., Nam, N. Q., Tu, N. V. (2023). Structural behavior of UHPC epoxy composite plate subjected to velocity impact loading. *Journal of Science and Technology in Civil Engineering (STCE) - HUCE*, 17(3):55–64.

[10] Hao, P. M., Thang, N. C., Thao, N. V., Tuan, N. V., Hai, L. N., Thuy, N. N., Man, N. X. (2022). Blast testing of ultra-high performance concrete fortifications using local materials. *Journal of Science and Technology in Civil Engineering (JSTCE) - HUCE*, 16(4):73–86.

[11] Niu, F., Liu, Y., Xue, F., Sun, H., Liu, T., He, H., Kong, X., Chen, Y., Liao, H. (2025). Ultra-high performance concrete: A review of its material properties and usage in shield tunnel segment. *Case Studies in Construction Materials*, 22:e04194.

[12] Que, Z., Tang, J., Wei, H., Zhou, A., Wu, K., Zou, D., Yang, J., Liu, T., De Schutter, G. (2024). Predicting the tensile strength of ultra-high performance concrete: New insights into the synergistic effects of steel fiber geometry and distribution. *Construction and Building Materials*, 444:137822.

[13] Su, X., Ren, Z., Li, P. (2024). Review on physical and chemical activation strategies for ultra-high performance concrete (UHPC). *Cement and Concrete Composites*, 149:105519.

[14] Wang, D., Zhang, G., Chen, H., Hu, Y., Qi, D., Chen, H. (2025). Investigation on mechanical properties of expansive lightweight aggregate ultra-high-performance concrete-filled steel tube short columns: Axial compression and interfacial bonding performance. *Case Studies in Construction Materials*, 22:e04288.

[15] Yoo, D.-Y., Banthia, N., Yoon, Y.-S. (2024). Recent development of innovative steel fibers for ultra-high-performance concrete (UHPC): A critical review. *Cement and Concrete Composites*, 145:105359.

[16] Ge, W., Zhang, Z., Ashour, A., Jiang, H., Chan, Y. W. S. (2025). Seismic performance of SFCBs reinforced UHPC-filled steel tube composite columns: Test, modeling and theoretical analysis. *Journal of Building Engineering*, 104:112166.

[17] Li, P., Cao, B., Ren, Z., Abbas, M. A., Jiang, J., Li, Q. (2024). Comparative study on axially-loaded round-cornered square high-strength steel tube confined UHPC columns. *Case Studies in Construction Materials*, 20:e02903.

[18] Li, P., Xu, L., Abbas, M. A., Ren, Z. (2023). Material synergy and parameter optimization of axially-loaded circular UHPC-filled steel tubes. *Journal of Constructional Steel Research*, 202:107772.

[19] Wu, F., Xu, L., Zeng, Y., Yu, M., Li, B. (2023). Behavior of CA-UHPC filled circular steel tube stub columns under axial compression. *Journal of Constructional Steel Research*, 211:108204.

[20] Zhao, Z., Wei, Y., Wang, G., Zhang, Y., Lin, Y. (2023). Axial compression performance of square UHPC-filled stainless-steel tubular columns. *Construction and Building Materials*, 408:133622.

[21] Xiong, M.-X., Xiong, D.-X., Liew, J. R. (2017). Axial performance of short concrete filled steel tubes with high- and ultra-high- strength materials. *Engineering Structures*, 136:494–510.

[22] EN 1994-1-1:2004 (2004). *Eurocode 4: Design of composite steel and concrete structures*. European Committee for Standardization, pp. 1998-1.

[23] Chen, H., Liao, F., Yang, Y., Ren, Y. (2023). Behavior of ultra-high-performance concrete (UHPC) encased concrete-filled steel tubular (CFST) stub columns under axial compression. *Journal of Constructional Steel Research*, 202:107795.

[24] Li, W., Zhu, M., Li, G., Hu, Y., Wang, B., Cao, Y., He, W., Li, H., Tang, Z., Zhang, Y. (2024). Influence of Compressive Strength and Steel-Tube Thickness on Axial Compression Performance of Ultra-High-Performance Concrete-Filled Stainless-Steel Tube Columns Containing Coarse Aggregates. *Buildings*, 14(11):3605.

[25] Lai, D., Chen, Y., Liao, F., Qiu, H., Xu, C., Zheng, R. (2024). UHPC-encased CFST composite columns under lateral impact: An experimental investigation. *Journal of Constructional Steel Research*, 222: 108948.

[26] Cheng, B., Wang, W., Li, J., Huang, J., Chen, H. (2023). Mechanical Properties of Full-Scale UHPC-Filled Steel Tube Composite Columns under Axial Load. *Materials*, 16(13):4860.

[27] Cai, H., Deng, F., Yan, Y. (2022). Nonlinear analysis on the static and cyclic behaviors of UHPC filled rectangular steel tube columns. *KSCE Journal of Civil Engineering*, 26(3):1316–1328.

[28] Patel, V. I., Hassanein, M. F., Thai, H.-T., Al Abadi, H., Elchalakani, M., Bai, Y. (2019). Ultra-high strength circular short CFST columns: Axisymmetric analysis, behaviour and design. *Engineering Structures*, 179:268–283.

[29] Han, L.-H. (2024). *Theory of concrete-filled steel tubular structures*. Springer.

[30] Tao, Z., Wang, Z.-B., Yu, Q. (2013). Finite element modelling of concrete-filled steel stub columns under axial compression. *Journal of Constructional Steel Research*, 89:121–131.

[31] Lam, L., Teng, J. G. (2003). Design-oriented stress–strain model for FRP-confined concrete. *Construction and Building Materials*, 17(6–7):471–489.

[32] Chen, S., Zhang, R., Jia, L.-J., Wang, J.-Y., Gu, P. (2018). Structural behavior of UHPC filled steel tube columns under axial loading. *Thin-Walled Structures*, 130:550–563.